Available online at www.sciencedirect.com
SCIENCE DIRECT
Catalysis Today 104 (2005) 7–17
CATALYSIS TODAY
www.elsevier.com/locate/cattod

Thermographical observation of catalyst bed temperature in oxidative steam reforming of methane over Ni supported on α-alumina granules: Effect of Ni precursors

Baitao Li, Ritsuko Watanabe, Kenji Maruyama, Kimio Kunimori, Keiichi Tomishige *

Institute of Materials Science, University of Tsukuba, 1-1-1, Tennodai, Tsukuba, Ibaraki 305-8573, Japan

Available online 7 April 2005

Abstract

Catalyst bed temperature during the oxidative steam reforming of methane over α-Al_2O_3-supported Ni catalysts, prepared from three different precursors (nickel nitrate, nickel acetate and nickel chloride), was studied with infrared thermograph at 1073 K. It was found that the temperature near the catalyst bed inlet increased with decreasing *W*/*F* (contact time *W*/*F*: *W* (g): catalyst weight, *F* (mol/h): total flow rate of the introduced gases) in oxidative steam reforming of methane. It is thought that the bed temperature profile is influenced by the catalytic activities of methane combustion and reforming reactions. However, in the case of Ni/α-Al_2O_3, it was intriguing to find that the highest bed temperature was not so influenced by the metal loading, dispersion and preparation method. The reason for this interesting result is because the catalyst with higher combustion activity has higher reforming activity. Consequently, higher temperature, which is caused by high combustion activity, is compensated to the similar level by means of endothermic reforming.

Keywords: Ni catalysts; Precursor; Methane; Reforming; Combustion; Temperature profile; Thermography

1. Introduction

Steam reforming of methane (Eq. (1)) is an important and economical industrial technology for the production of synthesis gas [1]. Because methane conversion with steam is a highly endothermic reaction, it is necessary to heat the catalyst bed from outside the reactor. In general, the internal heating is more energy-efficient than the external heating. From this viewpoint, the process of autothermal reforming of methane has been developed [2].

$$CH_4 + H_2O \rightarrow CO + 3H_2, \quad \Delta H^0_{298} = 206\,kJ/mol \qquad (1)$$

In the autothermal reforming of methane, the steam reforming of methane is combined with noncatalytic partial oxidation of methane (Eq. (2)).

$$CH_4 + \tfrac{1}{2}O_2 \rightarrow CO + 2H_2, \quad \Delta H^0_{298} = -36\,kJ/mol \qquad (2)$$

Partial oxidation of methane is an exothermic reaction, as shown above. The heat from the noncatalytic partial oxidation of methane is supplied to the catalyst bed for the steam reforming. As an alternative, oxidative steam reforming of methane is another economical syngas production method, in which catalytic combustion of methane (Eq. (3)) is combined with steam (Eq. (1)) and/or CO_2 (Eq. (4)) reforming of methane.

$$CH_4 + 2O_2 \rightarrow CO_2 + 2H_2O, \quad \Delta H^0_{298} = -803\,kJ/mol \qquad (3)$$

$$CH_4 + CO_2 \rightarrow CO + 3H_2, \quad \Delta H^0_{298} = 247\,kJ/mol \qquad (4)$$

Because the combustion reaction proceeds more rapidly than the reforming reaction, it usually proceeds over the catalyst near the bed inlet, while the reforming reaction takes place over the catalyst bed after oxygen is consumed [3,4]. Therefore, at the catalyst bed inlet the temperature in the combustion zone is expected to be very high, while it decreases at the rear part because of the endothermic reforming reaction. As a result, a large temperature gradient will appear in the catalyst bed during the catalytic partial oxidation of methane [3,5–7]. In addition, the hot spot, one of the main difficulties in operating the partial oxidation [8–11], is still a common problem during the oxidative reforming process. In order to

* Corresponding author. Tel.: +81 29 853 5030; fax: +81 29 853 5030.
E-mail address: tomi@tulip.sannet.ne.jp (K. Tomishige).

0920-5861/$ – see front matter © 2005 Elsevier B.V. All rights reserved.
doi:10.1016/j.cattod.2005.03.037

inhibit the hot spot occurrence, several studies have been recently carried out on the partial oxidation and methane reforming using the fluidized bed reactor [12–18]. It has been found that in the fluidized bed reactor the heat transfer from the exothermic region to the endothermic zone was promoted and the hot spot formation was effectively inhibited; as a result, the stability and safety of the operation were successfully achieved. However, in the fluidized system, attrition of the catalyst particles is another serious problem. Therefore, the fix-bed system is usually promising.

Considerable efforts have been devoted to manufacturing synthesis gas by combination process, such as investigation on the effects of steam and CO_2 addition on partial oxidation of methane and the effect of O_2 addition on steam or dry reforming of methane [8–11,19–27]. In the oxidative steam reforming reaction, the combustion and the reforming of methane take place together over the same catalyst bed; this reaction coupling brings synergic heat effect, resulting in different temperature profiles. It has been found that Pt catalysts are very effective in the oxidative steam reforming reaction from the temperature profile measurement [8–11]. Furthermore, in our recent paper [28], we reported the thermographical results over α-Al_2O_3 granules-supported Rh, Pt and Pd catalysts, where Rh/α-Al_2O_3 catalyst exhibited a comparatively lower temperature profile than Pt and Pd catalyst. The reason for the significant temperature difference is because that Rh is superior in the reforming activity but with substantially low combustion activity, which leads to an effective overlap of the reforming and combustion zones to inhibit the hot spot formation. However, noble metals such as Pt, Pt and Rh are not suitable components because of their limited availability and high cost. Therefore, the development of Ni catalyst for the oxidative steam reforming of methane has been extensively attempted [29–33]. It is supposed that Ni catalysts exhibit much higher temperature gradient than noble metal catalysts such as Pt and Rh. This is because that Pt and Rh have much lower oxygen affinity than that of Ni [34]; on the contrary, Ni is easily oxidized by the contact with oxygen and loses the reforming activity [35].

In this article, we studied the temperature profile over the catalyst bed and the activity test in oxidative steam reforming of methane, methane combustion and methane reforming with steam and CO_2, especially the effects of Ni precursor and loading amount were investigated. Catalyst characterization was also performed by means of X-ray diffraction (XRD), H_2 temperature-programmed reduction (H_2-TPR) and the measurement of H_2 adsorption. The correlation between catalyst structure and catalytic performance as well as temperature profile was also carefully discussed.

2. Experimental

2.1. Catalyst preparation

All catalysts were prepared by the conventional impregnation method. Alumina support was prepared by the calcination of JRC-ALO-1 (Catalysis Society of Japan, diameter of 2–3 mm, 143 m^2/g) in air at 1473 K for 3 h. X-ray diffraction confirmed its structural change from γ-Al_2O_3 to α-Al_2O_3, as shown later. The surface area of the calcined alumina was determined to be 7 m^2/g. Alumina-supported nickel catalysts (Ni/α-Al_2O_3) were prepared by impregnating calcined α-Al_2O_3 granules with aqueous solution of $Ni(NO_3)_2{\cdot}6H_2O$, $Ni(CH_3COO)_2{\cdot}4H_2O$, $NiCl_2{\cdot}6H_2O$ (Wako Pure Chemical Industries Ltd., 99.9%), respectively. After the impregnation, the catalysts were dried at 383 K for 12 h and calcined at 773 K for 3 h in air. Ni loading amount was denoted in the parentheses, for example, Ni (0.4), which represents that the weight percent of Ni catalyst is 0.4 wt.%. Catalyst, prepared by $Ni(NO_3)_2{\cdot}6H_2O$, $Ni(CH_3COO)_2{\cdot}4H_2O$ and $NiCl_2{\cdot}6H_2O$, is denoted as Ni-N, Ni-A and Ni-C, respectively.

2.2. Activity test and thermographical observation

The reforming of methane reaction was carried out under atmospheric pressure using flow-type quartz reactor (8 mm o.d., 6 mm i.d.). Schematic diagram of the fixed-bed reactor is illustrated in Fig. 1A. The reaction temperature was monitored by a chromel–alumel thermocouple covered with a quartz thermowell (1.5 mm i.d.), which was located at the outlet of the catalysts bed. An electronic furnace was equipped with the thermo-controller and it had a window (15 mm × 15 mm) for the observation of the temperature profile. The surface temperature was measured with IR thermography equipment (TH31, NEC San-ei Instruments Ltd.). The picture of the catalyst granules before the reaction at room temperature is shown in Fig. 1B(a); a thermographical image during a reaction is presented in Fig. 1B(b) as an example. The vertical temperature profile along the catalyst bed was obtained from the cross-section of the maximum temperature, except in the methane reforming with steam and CO_2, which was given from the endothermic profile with the cross-section through the minimum temperature.

The catalyst (0.14 g) was reduced in the hydrogen flow (30 ml/min, 100% H_2) at 1123 K for 0.5 h prior to the activity tests. After reduction, the catalyst bed was cooled down to the reaction temperature in Ar flow. Several kinds of partial pressure condition were tested and the details of the reaction conditions were described in each reaction result. All the reactant gases were purchased from Takachiho Trading Co. Ltd. in research grade, and they were used without further purification. Contact time W/F (W (g): catalyst weight; F (mol/h): total flow rate of the introduced gases) was adjusted in the range of 0.12–1.20 g h/mol (GHSV = 100,000–10,000 h^{-1}) under the constant catalyst weight. The reactants and the products, which were collected by a syringe from the sampling port, were analyzed by gas chromatography (GC) after water condensation. The concentration of CO, CO_2 and CH_4 in the effluent gas was accomplished by FID-GC equipped with a methanator using a stainless steel column packed with

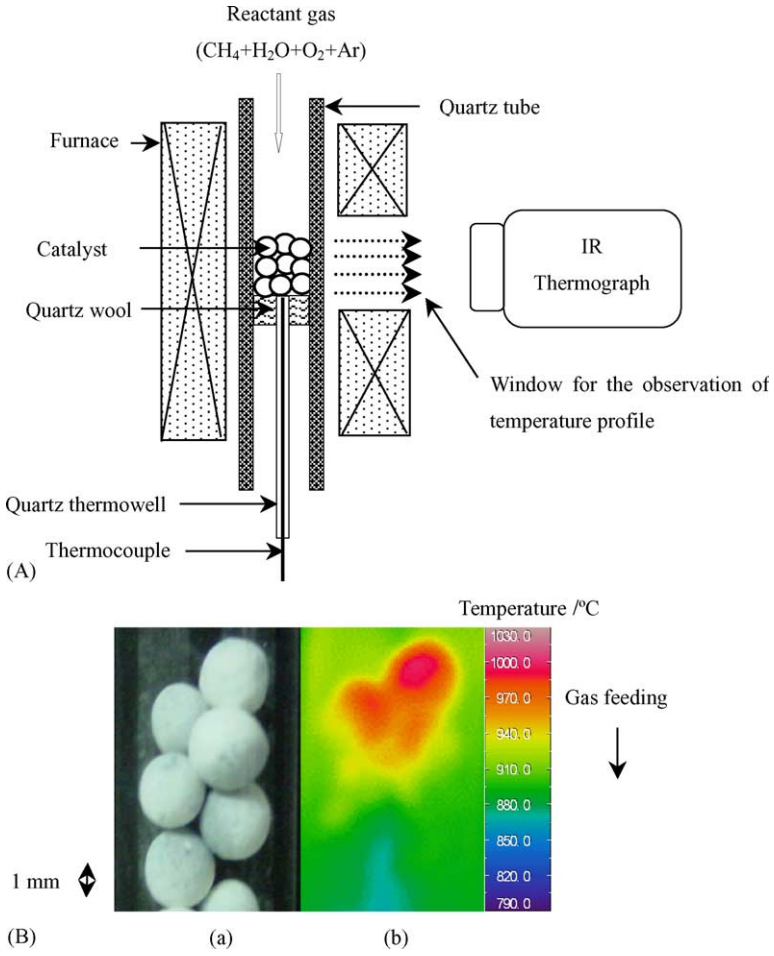

Fig. 1. (A) Schematic diagram of the fixed-bed reactor in the reforming of methane and the method of temperature profile observation and (B) picture of catalyst granules in the quartz glass tube: (a) before reaction and (b) one example of thermographical image.

Porapak N; the concentration of H_2 was determined by TCD-GC using a stainless steel column packed with a molecular sieve 13×. In the syngas production by methane reforming, the carbon deposition is a serious problem which causes catalyst deactivation, reactor plugging and destroy of the catalysts [36,37]. In the experiment, we carried out the catalytic test for 0.5 h under each reaction condition. After the reaction, we measured the amount of carbon deposition and found the amount was negligible. Therefore, the effect of deposited carbon was neglected over all the catalysts in this paper.

2.3. Characterization of catalysts

The fresh catalysts were characterized by chemisorption experiment, which was carried out in a high-vacuum system by volumetric methods (dead volume: 27 ml). Prior to the adsorption measurement, the catalysts were reduced with H_2 flow at 1123 K for 0.5 h in the fixed-bed reactor, which was used in the activity test. The pre-treated catalyst was transferred to the vacuum line under air atmosphere. In the vacuum line, H_2 reduction at 773 K for 1 h and evacuation at 723 K for 1 h were carried out. After the pretreatments, the adsorption amount of H_2 was measured at room temperature and the equilibrium pressure of the gas was about 2.7 kPa.

Power X-ray diffraction patterns of the reduced samples (H_2 flow, 1123 K, 0.5 h) were recorded on a Philips X'pert diffractometer, using Cu Kα ($\lambda = 0.154$ nm) generated at 40 kV and 20 mA. Scanning was conducted over the range of $2\theta = 5–75^\circ$.

Temperature-programmed reduction (TPR) experiments were carried out in a fixed-bed reactor equipped with TCD-GC. Reduction profiles were obtained by passing 5% H_2/Ar at a rate of 30 ml/min through the pre-calcined sample (weight around 50 mg). The temperature was increased from the room temperature to 1123 K with a heating rate of 10 K/min. H_2 consumption was accurately measured from the integrated peak area of the reduction profiles.

3. Results and discussion

3.1. Effect of the granule size

The purpose of this experiment is to investigate the effect of the particle size on the temperature profile during the

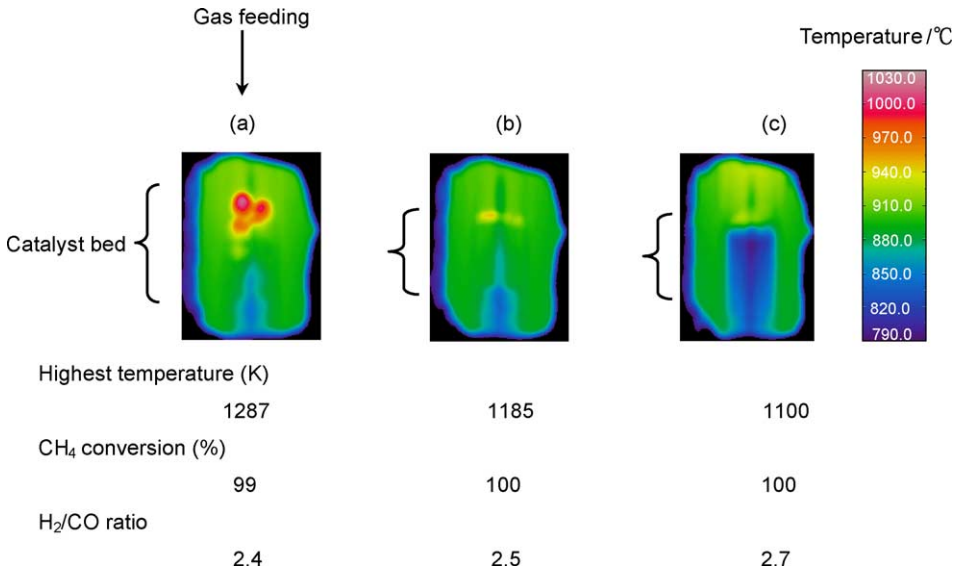

Fig. 2. Comparison of IR thermography over Ni (10.6)-N with different morphology in autothermal reforming of methane: (a) granule (2–3 mm); (b) 150–250 μm; (c) 75–150 μm. Reaction conditions: $CH_4/H_2O/O_2/Ar = 40/30/20/10$, $W/F = 0.24$ g h/mol, temperature 1123 K, total pressure 0.1 MPa, catalyst weight 0.14 g and H_2 pretreatment at 1123 K.

oxidative reforming of methane ($CH_4/H_2O/O_2/Ar = 40/30/20/10$) over Ni (10.6)-N catalyst. The catalysts with small granule size were prepared by crushing and sieving the Ni supported on α-Al_2O_3 granules. The loading of Ni on α-Al_2O_3 granules was homogenous and the concentration of nickel species was constant in the granule judging from the observation of the color inside. Therefore, the state of nickel in the catalyst granules with different size was thought to be identical.

Fig. 2 shows the thermographical image, methane conversions and H_2/CO in oxidative reforming of methane over Ni (10.6)-N with three different sizes at $W/F = 0.24$ g h/mol. Methane conversion was slightly higher over the catalysts with smaller granule size, which indicates that methane conversion is related to the outer surface area of the particles. Furthermore, the highest temperature in the catalyst bed was strongly dependent on the particle size; it was much higher over the catalysts with larger particle size. Especially, the hot spot was clearly observed over the catalyst granules with 2–3 mm Ø. As reported previously, in the case of oxidative steam reforming of methane, the highest temperature in the catalyst bed is related to the combustion and reforming activities and the overlap of two reaction zones [8–11]. The reforming reaction is enhanced more significantly over the catalysts with larger outer surface area; therefore, the overlap of reaction zones is promoted on the catalyst with small granule size.

However, from the practical and industrial viewpoint, the catalyst with large size is preferred, especially under the condition of high flow rate. The powder catalyst is not applicable because of a pressure difference between the catalyst bed inlet and outlet. In fact, in our experiment, it was very difficult to feed the reactant gases at low W/F condition such as 0.16 g h/mol over 75–150 μm catalyst because of the high pressure difference. On the other hand, compared with the conventional steam reforming which requires external heat supplying, oxidative steam reforming of methane improves the energy efficiency by the internal heat supply; this will result in considerably higher syngas productivity through high feeding rate of reactant gases. Therefore, it is important to obtain the temperature profile of the catalysts with larger granule size under high flowing rate condition in order to observe the hot spot formation, which is one of the most serious problems in oxidative steam reforming of methane. As described below, we carried out the experiment using granule catalysts with 2–3 mmØ.

3.2. Catalyst characterization

The TPR were carried out to compare the reducibility of the nickel oxide on the fresh catalyst. The TPR profiles of the samples are shown in Fig. 3. H_2 consumption was estimated by the peak area of TCD-GC; the signal intensity was normalized by total amount of Ni contained in the catalysts. The reduction degree (Ni^0/Ni_{total}) was calculated on the basis of the equation: $H_2 + NiO \rightarrow Ni + H_2O$; the results are presented in Table 1. The reduction degree of all the catalysts was determined to be close to 100%, indicating Ni was completely reduced at 1123 K. For Ni-N and Ni-A, the TPR peak, which was assigned to the reduction of NiO, was observed at 723 K [42,43], while it was at about 670 K over Ni-C. It has been reported that the interaction between nickel oxide and support can affect the reduction temperature [44]. In the case of the weak interaction, nickel species can be reduced at lower temperature than that of the strong interaction. Furthermore, for the catalysts with high loading, the peak was found to shift to lower temperature. It is thought that nickel species with larger particle size have

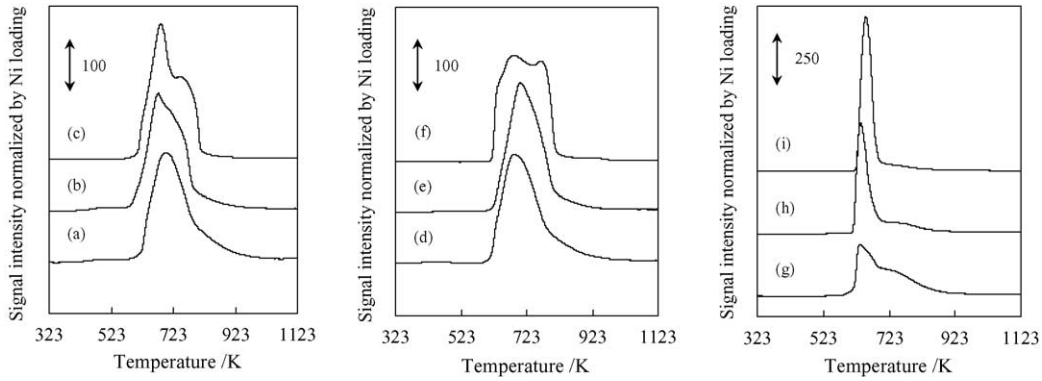

Fig. 3. Temperature-programmed reduction (H_2-TPR) profiles over the supported nickel catalysts: (a) Ni (0.4)-N; (b) Ni (0.9)-N; (c) Ni (2.6)-N; (d) Ni (0.4)-A; (e) Ni (0.9)-A; (f) Ni (2.6)-A; (g) Ni-(0.4) C; (h) Ni (0.9)-C; (i) Ni (2.6)-C. Conditions: temperature range 293–1123 K, 5% H_2/Ar (30 ml/min) and heating rate 10 K/min.

small interface with the support surface; this will lead to a weak interaction between support and the nickel metal, thus makes the nickel particles easy to reduce. Therefore, it is deduced that the particle size of nickel oxide will affect the reduction temperature in TPR profiles; the larger the particle size, the lower the reduction temperature.

Fig. 4 shows the XRD patters of the catalysts after H_2 treatment. Over the catalyst, Ni (2.6)-N, Ni (2.6)-A and Ni-C, the peaks assigned to Ni metal ($2\theta = 44.5^\circ$) [31,44] were observed, although the signal intensity was not so strong except Ni (2.6)-C. On the basis of XRD patterns, the particle size of Ni was calculated and the results are shown in Table 1. However, the XRD peak could not be observed over some samples. In order to estimate the particle size on the catalysts with lower Ni loading, on which XRD peaks due to Ni metal were not observed, we measured the amount of H_2 adsorption and the results are also summarized in Table 1. The average particle size given from XRD pattern was almost consistent with that calculated from H_2 adsorption measurement. It is seen that the particle size of Ni metal increased with the rise of Ni content. Furthermore, the particle size of Ni-N and Ni-A was similar to each other and both of them are smaller than that of Ni-C. This tendency can be explained by the TPR profile. NiO particle formed from $NiCl_2$ exhibited lower reduction peak, and this means that the interaction of NiO with support surface is rather weak and the particle size of NiO is very large.

It is a general rule that particle size with 9 nm should be observed from XRD patterns; however, in our case no diffraction peak was found for Ni (0.4)-N and Ni (0.4)-A catalysts. It is thought that the concentration of Ni particles was so low that the diffraction intensity was beyond the detection level.

3.3. Oxidative steam reforming of methane

Oxidative steam reforming reaction was carried out over various supported Ni catalysts derived from different Ni precursors under the partial pressure of $CH_4/H_2O/O_2/Ar = 40/30/20/10$ at 1073 K. Catalyst performance at $W/F = 0.40$ g h/mol is shown in Table 2. It is clearly seen that methane conversion over Ni-A and Ni-N with various Ni content was almost in the same level, which was close to the equilibrium. The results indicate that these two catalysts

Table 1
Characterization results of the various Ni catalysts

Precursor	Catalyst	H_2 chemisorption H/Ni_{total}[a] (%)	Particle size of Ni (nm)		Reduction degree Ni^0/Ni_{total}[b] (%)
			Adsorption[c]	XRD[d]	
$Ni(NO_3)_2$	Ni (0.4)-N	10.9	9	–	101
	Ni (0.9)-N	8.0	12	–	102
	Ni (2.6)-N	5.8	17	19	100
$Ni(CH_3COO)_2$	Ni (0.4)-A	11.2	9	–	105
	Ni (0.9)-A	9.3	10	–	102
	Ni (2.6)-A	5.7	17	19	102
$NiCl_2$	Ni (0.4)-C	2.6	38	34	103
	Ni (0.9)-C	1.6	59	62	102
	Ni (2.6)-C	1.2	82	77	98

[a] Total (reversible and irreversible) chemisorption at 298 K.
[b] Determined by H_2-TPR profiles.
[c] Average particle size (average volume–area) based on H_2 adsorption amount [38,39].
[d] Calculated from Scherrer equation, using the half-width at half-height of the strong intensity metal peak [40,41]. Sample was pretreated at hydrogen flow, 1123 K and 0.5 h.

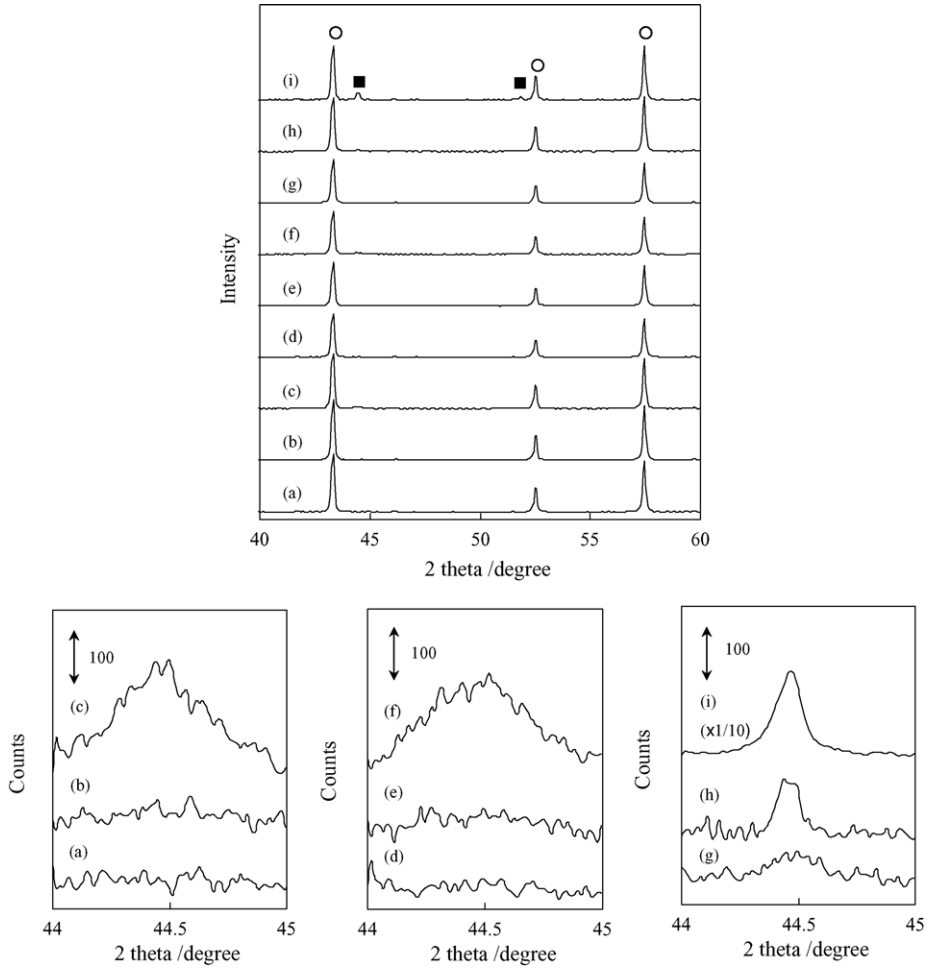

Fig. 4. XRD patterns of Ni catalysts with different metal loading amounts (reduced in H_2 flow, 1123 K, 30 min): (a) Ni (0.4)-N; (b) Ni (0.9)-N; (c) Ni (2.6)-N; (d) Ni (0.4)-A; (e) Ni (0.9)-A; (f) Ni (2.6)-A; (g) Ni (0.4)-C; (h) Ni (0.9)-C; (i) Ni (2.6)-C ((■) Ni and (○) α-Al_2O_3).

have very high catalytic activity. In contrast, methane conversion over Ni-C was lower than that over Ni-N and Ni-A, which was supported by its low metal dispersion in the characterization results.

Fig. 5 shows the effect of *W/F* on the thermographical images over Ni (0.4)-C in oxidative steam reforming of methane. At *W/F* = 1.20 g h/mol, almost no exothermic zone was observed. In the range of *W/F* = 0.12–0.80 g h/mol, the catalyst inlet temperature increased with decreasing *W/F*. Furthermore, at lower *W/F*, the hot zone spread out downstream. These results indicate that the hot spot easily occurs under the high flow rate condition (low *W/F*).

The effect of *W/F* on the temperature profiles over nine catalysts in the oxidative steam autothermal reforming is summarized in Fig. 6. It is clearly observed that the bed temperature increased with decreasing *W/F* over all the catalysts. Over Ni loading amount = 2.6 wt.% and under *W/F* = 0.12 g h/mol, the highest temperature over Ni-C was 1333 K, that over Ni-N was 1273 K and it was only 1233 K for Ni-A, indicating that the order of the bed temperature over the employed catalysts increases as follows: Ni-A < Ni-N < Ni-C.

Temperature profile as well as the methane conversion is extremely important in manufacturing synthesis gas in the oxidative steam reforming of methane. The formation of

Table 2
Comparison of the catalyst performance over various Ni catalysts in oxidative steam reforming of methane

Precursor	Catalyst	CH_4 conversion (%)	H_2/CO
Ni $(NO_3)_2$	Ni (0.4)-N	97	2.7
	Ni (0.9)-N	97	2.8
	Ni (2.6) N	98	2.6
Ni $(CH_3COO)_2$	Ni (0.4)-A	96	2.8
	Ni (0.9)-A	97	2.7
	Ni (2.6)-A	98	2.6
$NiCl_2$	Ni (0.4)-C	92	2.8
	Ni (0.9)-C	94	2.8
	Ni (2.6)-C	93	2.8
Equilibrium		>99	2.8

Reaction conditions: $CH_4/H_2O/O_2/Ar$ = 40/30/20/10, *W/F* = 0.40 g h/mol, temperature 1073 K, total pressure 0.1 MPa, catalyst weight 0.14 g and H_2 pretreatment at 1123 K. The loading amount of Ni (wt.%) is indicated in the parentheses.

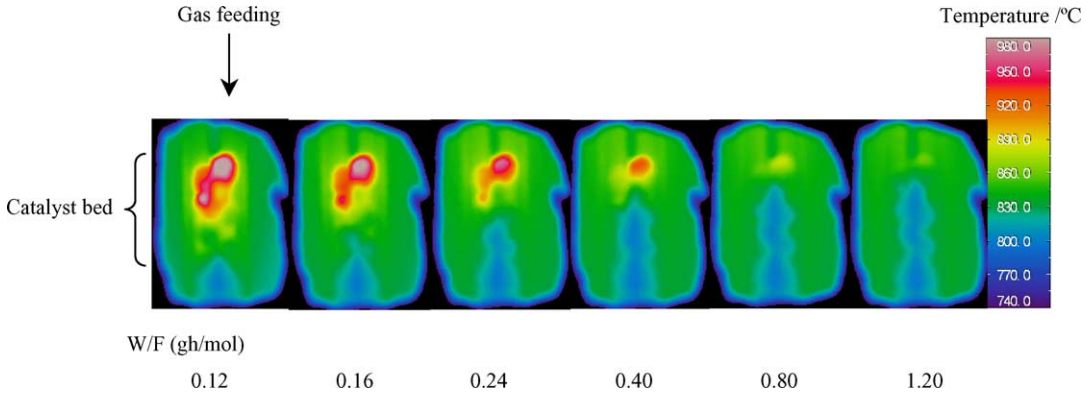

Fig. 5. IR thermography over Ni (0.4)-C in oxidative steam reforming of methane. Reaction conditions: $CH_4/H_2O/O_2/Ar = 40/30/20/10$, temperature 1073 K, total pressure 0.1 MPa, catalyst weight 0.14 g and H_2 pretreatment at 1123 K.

high-temperature section (hot spot) in the catalyst bed affects the aggregation of Ni metal particle and the sintering of support material. Consequently, the ideal catalyst design for the inhibition of hot spot formation is very necessary and attractive from the industrial point of view. As reported previously, oxidative steam reforming of methane consists of methane combustion and reforming of methane with steam and CO_2. Therefore, the highest bed temperature during this process is influenced and determined by both the combustion and the reforming activities. Furthermore, the overlap of combustion and reforming zones is also important. Based on the above reasons, we investigated the temperature profiles and catalytic performance of methane reforming (without using oxygen) and combustion individually.

3.4. Methane reforming with steam and CO_2

In the reforming of methane with steam and CO_2, oxygen was not introduced, and the performance of sole reforming reaction was investigated. The partial pressure was $CH_4/CO_2/H_2O/O_2/Ar = 30/10/50/0/10$, which corresponds to the gas composition when methane combustion only proceeded under $CH_4/H_2O/O_2/Ar = 40/30/20/10$ (the partial pressure for oxidative steam reforming described in the previous section). Table 3 lists the catalyst performance in terms of

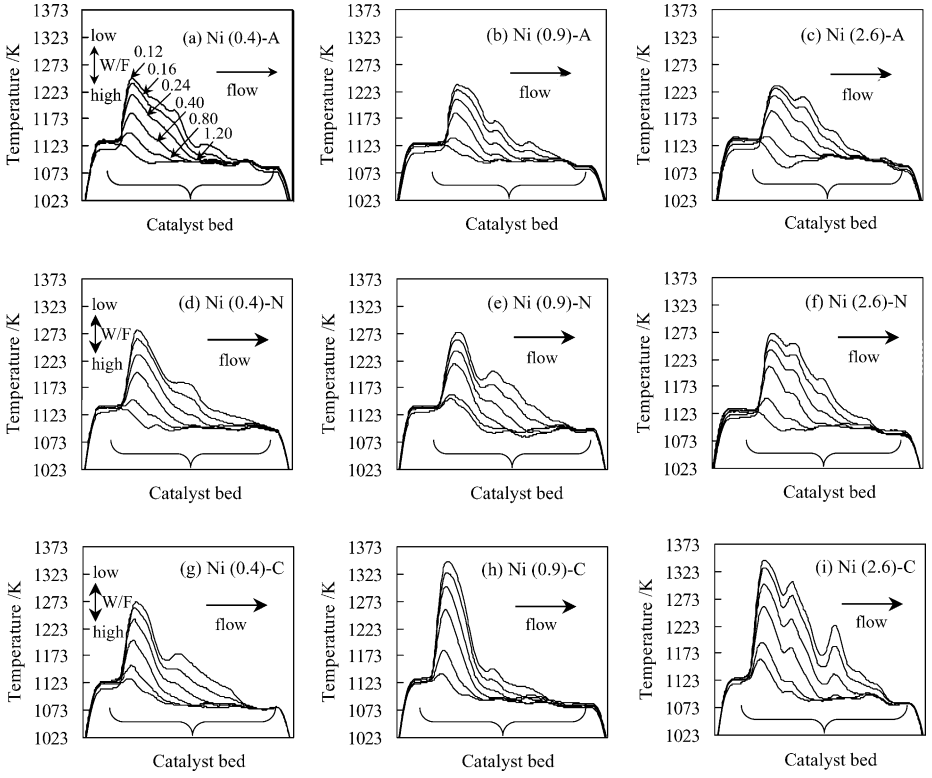

Fig. 6. Temperature profiles over Ni catalysts in oxidative steam reforming of methane. Reaction conditions: $CH_4/H_2O/O_2/Ar = 40/30/20/10$, temperature 1073 K, total pressure 0.1 MPa, catalyst weight 0.14 g and H_2 pretreatment at 1123 K.

Table 3
Comparison of the catalyst performance over various Ni catalysts in methane reforming with steam and CO_2

Precursor	Catalyst	CH_4 conversion (%)	H_2/CO	Lowest bed temperature[a] (K)
Ni $(NO_3)_2$	Ni (0.4)-N	82	3.5	993
	Ni (0.9)-N	84	3.3	993
	Ni (2.6)-N	90	3.0	955
Ni $(CH_3COO)_2$	Ni (0.4)-A	84	3.3	1009
	Ni (0.9)-A	86	3.2	980
	Ni (2.6)-A	88	3.1	966
$NiCl_2$	Ni (0.4)-C	76	3.4	993
	Ni (0.9)-C	80	3.3	987
	Ni (2.6)-C	78	3.3	971
Equilibrium		>99	3.0	–

Reaction conditions: $CH_4/CO_2/H_2O/O_2/Ar$ = 30/10/50/0/10, W/F = 0.40 g h/mol, temperature 1073 K, total pressure 0.1 MPa, catalyst weight 0.14 g and H_2 pretreatment at 1123 K.
[a] Lowest bed temperature observed in the thermographical image.

methane conversion and H_2/CO ratio and the lowest bed temperature over various Ni catalysts in methane reforming with steam and CO_2. It is clear that the tendency in methane conversion is almost consistent with that in oxidative steam reforming. Ni-A and Ni-N gave a litter higher methane conversion than Ni-C. Methane conversion in the reforming reaction was much lower than that in oxidative steam reforming of methane over each catalyst. This is because of the difference in the catalyst bed temperature. The bed temperature was much lower in the methane reforming with steam and CO_2 due to the endothermic reaction. Furthermore, lower methane conversion enhanced H_2/CO ratio via water gas shift reaction under high partial pressure of steam. Fig. 7 shows an example thermography over Ni (0.4)-C in methane reforming with steam and CO_2. Compared to the thermographical image of oxidative reforming of methane (Fig. 5), the catalyst bed temperature was much lower and the part except the catalyst bed was much higher. Low catalyst bed temperature is due to the endothermic reforming reaction. High-temperature part corresponds to high furnace temperature, which was controlled by the thermocouple at the bed outlet. The lowest temperatures found from the thermographical images at W/F = 0.40 g h/mol are also listed in Table 3. In most cases, higher methane conversion leads to lower bed temperature.

3.5. Combustion plus reforming of methane reaction

Considering that oxidative steam reforming of methane is a combination of methane combustion and reforming, we investigated the performance of complete methane combustion and the promoting effect of reforming gas. In order to evaluate the performance in methane combustion, the partial pressure ratio of $CH_4/H_2O/O_2/Ar$ = 10/0/20/70 was applied. Furthermore, the performance was also tested under $CH_4/H_2O/O_2/Ar$ = 20/10/20/50, which is the sum of reforming gas (CH_4/H_2O = 10/10) and combustion gas (CH_4/O_2 = 10/20). In the ratio of $CH_4/H_2O/O_2/Ar$ = 30/20/20/30 and 40/30/20/10, the feeding of reforming gas increased. Activity tests and temperature profile observation were obtained successively in the order of $CH_4/H_2O/O_2/Ar$ = 40/30/20/10 → 30/20/20/30 → 20/10/20/50 → 10/0/20/70. This order means that the catalysts are progressively exposed to the oxidative atmosphere after reductive atmosphere. During the measurement, the performance was stable over all the catalysts. Here, a series

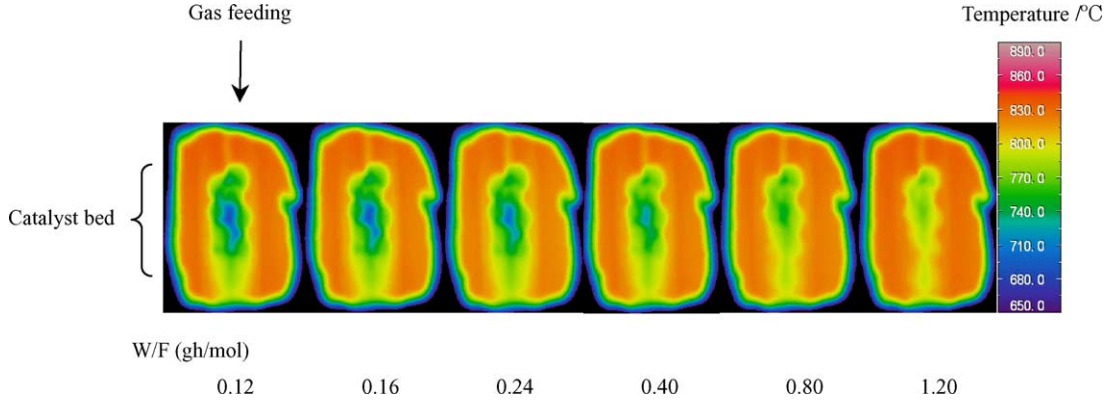

Fig. 7. IR thermography over Ni (0.4)-C in methane reforming with steam and CO_2. Reaction conditions: $CH_4/CO_2/H_2O/O_2/Ar$ = 30/10/50/0/10, temperature 1073 K, total pressure 0.1 MPa, catalyst weight 0.14 g and H_2 pretreatment at 1123 K.

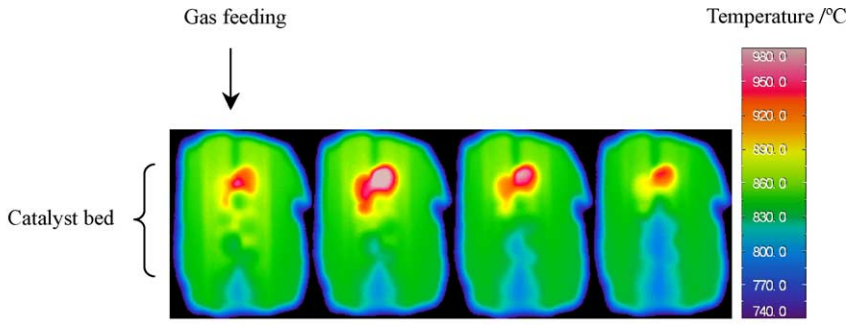

$CH_4/H_2O/O_2/Ar$	10/0/20/70	20/10/20/50	30/20/20/30	40/30/20/10
CH_4 conversion /%	83	96	94	92
H_2/CO ratio	-	2.7	2.8	2.8

Fig. 8. IR thermography over Ni (0.4)-C in combustion plus steam reforming of methane. Reaction conditions: temperature 1073 K, W/F = 0.40 g h/mol, total pressure 0.1 MPa, catalyst weight 0.14 g and H_2 pretreatment at 1123 K.

of the experiments are denoted as "combustion plus reforming reaction".

The example of thermographical image over Ni (0.4)-C is shown in Fig. 8. In the IR thermographical image under the reaction condition of methane combustion ($CH_4/H_2O/O_2$/Ar = 10/0/20/70), only a small hot zone was observed. In contrast, when the reforming gas was fed to the combustion gas ($CH_4/H_2O/O_2$/Ar = 20/10/20/50), a hot zone was observed clearly than that under the methane combustion condition. This suggests that Ni (0.4)-C exhibited higher combustion activity under $CH_4/H_2O/O_2$/Ar = 20/10/20/50 than under $CH_4/H_2O/O_2$/Ar = 10/0/20/70. This interesting behavior indicates that reforming gas or reforming atmosphere can dramatically enhance the combustion activity. When more reforming gas was further added to the combustion gas, the bed temperature decreased gradually since the contribution of the endothermic reforming became more obviously.

Fig. 9 shows the highest bed temperature over various Ni catalysts under four kinds of partial pressure in the combustion plus steam reforming of methane. In the case of $CH_4/H_2O/O_2$/Ar = 40/30/20/10, the highest temperature was located in the range of 1173–1273 K over all the catalysts. The temperature of Ni-N was about 1223 K, and that of Ni-A was about 1200 K, that of Ni (0.9)-C and Ni (2.6)-C was much higher. When the reforming gas decreased, the highest temperature increased over all the catalysts. Although this temperature jump is due to the decrease of endothermic contribution, the change of temperature was much dependent on the nature of the catalyst itself.

Table 4 lists the catalyst performance under four kinds of combustion plus reforming conditions. Under $CH_4/H_2O/O_2$/Ar = 40/30/20/10, methane conversion over Ni-N and Ni-A was beyond 95%, while it was not so high over Ni-C. This similar tendency in methane conversion was also observed under other conditions such as $CH_4/H_2O/O_2$/Ar = 30/20/20/30 and 20/10/20/50. In addition, when the partial pressure of reforming gas decreased, methane conversion increased gradually. This can be explained by the contribution of methane combustion increased and that of methane reforming decreased. However, under methane combustion ($CH_4/H_2O/O_2$/Ar = 10/0/20/70), methane conversion significantly decreased to be about 80%. The behavior in methane reforming under $CH_4/H_2O/O_2$/Ar = 20/10/20/50 → 10/0/20/70 was completely different from that under $CH_4/H_2O/O_2$/Ar = 40/30/20/10 → 30/20/20/30 → 20/10/20/50. This behavior is also supported by the thermographical observation, as shown in Fig. 8. The highest bed temperature increased under the condition of $CH_4/H_2O/O_2$/Ar = 40/30/20/10 → 30/20/20/30 → 20/10/20/50 over all the catalysts, which is because the decrease in the

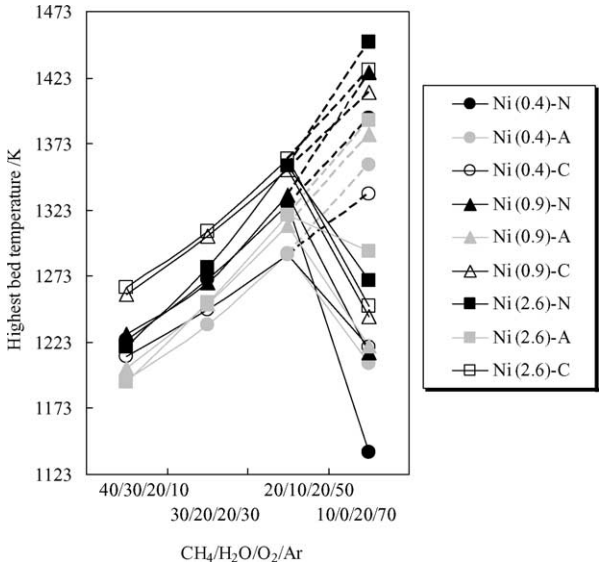

Fig. 9. Comparison of highest bed temperature over various Ni catalysts in the combustion plus steam reforming of methane (dotted line: the extrapolation data). Reaction conditions: temperature 1073 K, W/F = 0.40 g h/mol, total pressure 0.1 MPa, catalyst weight 0.14 g and H_2 pretreatment at 1123 K.

contribution of the reforming reaction results in the increase in the bed temperature. On the other hand, when the introduced gas was changed from $CH_4/H_2O/O_2/Ar = 20/10/20/50$ to 10/0/20/70, the highest bed temperature drastically decreased over all the catalysts. Generally, higher temperature part is formed over the catalysts with higher combustion activity; therefore, the thermographical results in Fig. 8 also indicate that methane combustion activity was considerably low, which was consistent with methane conversion (Table 4).

Judged from the result that methane conversion did not reach 100% under $CH_4/H_2O/O_2/Ar = 10/0/20/70$ and the oxygen partial pressure was not zero even at the outlet of the catalyst bed, it is deduced that the Ni catalyst is likely in the oxidized state. Therefore, we can deduce that in the experiment under $CH_4/H_2O/O_2/Ar = 10/0/20/70$, we actually evaluated the activity of methane combustion over the oxidized nickel catalyst. In fact, in the oxidative reforming of methane, methane combustion proceeds over the reduced catalyst; however, it would be very difficult to measure the methane combustion activity over reduced catalyst because Ni is easily oxidized. Therefore, in this paper, we estimated the combustion activity over reduced catalyst by the extrapolation, as shown in Fig. 9. The dotted line are the extrapolated data at $CH_4/H_2O/O_2/Ar = 10/0/20/70$ on the basis of $CH_4/H_2O/O_2/Ar = 40/30/20/10$, 30/20/20/30 and 20/10/20/50, assuming that the temperature jump is at the same interval when the reforming gas is decreased. One can find that the combustion activities of Ni (2.6)-C, Ni (0.9)-C, Ni (2.6)-N and Ni (0.9)-N are rather high. The slope of the line corresponds to the reforming ability; the inclined the line, the higher the reforming ability. According to Table 3, Ni-C catalysts gave lower methane conversion in methane reforming with steam and CO_2 than other Ni catalysts, which agrees with the slope in Fig. 9.

Fig. 10 shows the relation between the estimated highest bed temperature by the extrapolation in $CH_4/H_2O/O_2/Ar = 10/0/20/70$ and temperature difference between $CH_4/H_2O/O_2/Ar = 20/10/20/50$ and 40/30/20/10. All the points are based on the data in Fig. 9. The estimated highest bed temperature under $CH_4/H_2O/O_2/Ar = 10/0/20/70$ is corresponded to the combustion activity under the ideal reductive condition, where Ni metal is the active site of the combustion reaction. On the other hand, the temperature difference in $CH_4/H_2O/O_2/Ar = (20/10/20/50) - (40/30/20/10)$ is caused by the different contribution of steam reforming reaction, which also proceeds over Ni metal catalyst. In Fig. 10, both the combustion and reforming reactions can be controlled by the amount of Ni metal species on the catalyst. From this viewpoint, Fig. 10 reveals the relation between the reforming activity and the combustion activity under the reductive atmosphere, suggesting that the catalysts with high reforming activity have high combustion activity. Over the Ni catalysts investigated here, the reforming activity is almost proportional to the combustion activity, although the loading amount and particle size of Ni metal are considerably different. Therefore, the highest bed temperature in oxidative steam reforming of methane, which is influenced by reforming and combustion activities, exhibits no meaningful difference over the investigated Ni catalysts.

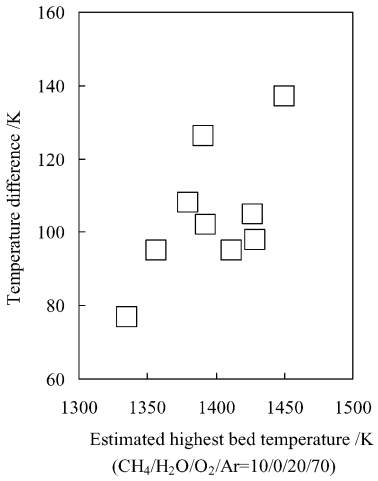

Fig. 10. Relation between the estimated highest bed temperature in $CH_4/H_2O/O_2/Ar = 10/0/20/70$ and temperature difference in $CH_4/H_2O/O_2/Ar = (20/10/20/50) - (40/30/20/10)$. Data are based on Fig. 9.

Table 4
Methane conversion and H_2/CO ratio in combustion plus reforming reaction

Catalyst	40/30/20/10[a]		30/20/20/30		20/10/20/50		10/0/20/70	
	CH_4 conversion (%)	H_2/CO	CH_4 conversion (%)	H_2/CO	CH_4 conversion (%)	H_2/CO	CH_4 conversion (%)	H_2/CO
Ni (0.4)-N	97	2.7	97	2.7	98	2.7	83	–
Ni (0.9)-N	97	2.8	97	2.5	98	2.4	83	–
Ni (2.6)-N	98	2.6	99	2.7	100	2.6	85	–
Ni (0.4)-A	96	2.8	97	3.0	98	2.5	80	–
Ni (0.9)-A	97	2.7	98	2.6	99	2.7	82	–
Ni (2.6)-A	98	2.6	99	2.6	99	2.4	87	–
Ni (0.4)-C	92	2.8	94	2.8	96	2.7	83	–
Ni (0.9)-C	94	2.8	96	2.7	97	2.6	84	–
Ni (2.6)-C	93	2.8	94	2.8	96	2.7	84	–

Reaction conditions: $W/F = 0.40$ g h/mol, temperature 1073 K, total pressure 0.1 MPa, catalyst weight 0.14 g and H_2 pretreatment at 1123 K.
[a] Gas composition $CH_4/H_2O/O_2/Ar$.

4. Conclusion

1. Temperature profiles of the catalyst bed during oxidative steam reforming of methane over Ni catalysts supported on α-Al_2O_3 granules were measured with infrared thermograph. High-temperature zone was observed near the catalyst bed inlet.
2. Highest temperature in the catalyst bed was much influenced by the size of the catalyst granules. When the size became smaller, the bed temperature was lower. In terms of hot spot observation and the practical aspect, the granule with 2–3 mmØ is thought to be suitable.
3. Ni catalysts supported on α-Al_2O_3 granules were prepared from nickel nitrate, nickel acetate and nickel chloride with the loading amount of Ni 0.4–2.6 wt.%. It was found the catalysts derived from the former two precursors were highly dispersed. In contrast, the dispersion of Ni from nickel chloride was much lower.
4. In oxidative steam reforming of methane, the highest bed temperature was not so different over various nickel catalysts prepared by various precursors with different loading.
5. From the results in combustion plus reforming reaction, we evaluated the combustion activity in reductive atmosphere. Based on the extrapolated result, it is deduced that the estimated combustion activity is almost proportional to the reforming activity. In this case, the catalysts led to a high bed temperature due to high combustion activity; however, high reforming activity decreased the bed temperature simultaneously. This is the reason why the highest bed temperature in oxidative steam reforming of methane did not change so much over various Ni catalysts.

Acknowledgements

We sincerely thank Japan Oil, Gas and Metals National Corporation (JOGMEC) and Chiyoda Corporation for financial supports.

References

[1] J.R. Rostrup-Nielsen, Catalysis: Science Technology, vol. 5, Spring-Verlag, New York, 1984.
[2] K. Aasberg-Petersen, J.-H. Bak Hansen, T.S. Christensen, I. Dybkjaer, P. Seier Christensen, C. Stub Nielsen, S.E.L. Winter Madsen, J.R. Rostrup-Nielsen, Appl. Catal. A Gen. 221 (2001) 379.
[3] E.P.J. Mallens, J.H.B.J. Hoebink, G.B. Marin, Catal. Lett. 33 (1995) 291.
[4] D. Dissanayaki, M.P. Rosynek, J.H. Lunsford, J. Phys. Chem. 97 (1993) 3644.
[5] K. Heitnes, S. Lingberg, O.A. Rokstad, A. Holmen, Catal. Today 24 (1995) 211.
[6] A.M. De Groote, G.F. Froment, Appl. Catal. A Gen. 138 (1996) 245.
[7] F. Basile, G. Fornasari, F. Trifiro, A. Vaccari, Catal. Today 64 (2001) 21.
[8] K. Tomishige, S. Kanazawa, M. Sato, K. Ikushima, K. Kunimori, Catal. Lett. 84 (2002) 69.
[9] K. Tomishige, S. Kanazawa, K. Suzuki, M. Asadullah, M. Sato, K. Ikushima, K. Kunimori, Appl. Catal. A Gen. 233 (2002) 35.
[10] K. Tomishige, S. Kanazawa, S. Ito, K. Kunimori, Appl. Catal. A Gen. 244 (2003) 71.
[11] K. Tomishige, M. Nurunnabi, K. Maruyama, K. Kunimori, Fuel Proc. Tech. 85 (2004) 1103.
[12] L. Garcia, A. Benedicto, E. Romeo, M.L. Salvador, J. Arauzo, R. Bilbao, Energy Fuel 16 (2002) 1222.
[13] K. Tomishige, Y. Matsuo, M. Asadullah, Y. Yoshinaga, Y. Sekine, K. Fujimoto, Acs. Sym. Ser. 809 (2002) 303.
[14] K. Opoku-Gyamfi, A.A. Adesina, Appl. Catal. A Gen. 180 (1999) 113.
[15] K. Tomishige, Y. Matsuo, Y. Yoshinaga, Y. Sekine, M. Asadullah, K. Fujimoto, Appl. Catal. A Gen. 223 (2002) 225.
[16] K. Tomishige, Y. Matsuo, Y. Sekine, K. Fujimoto, Catal. Commun. 2 (2001) 11.
[17] Y. Matsuo, Y. Yoshinaga, Y. Sekine, K. Tomishige, K. Fujimoto, Catal. Today 63 (2000) 439.
[18] K. Tomishige, Catal. Today 89 (2004) 405.
[19] A. Effendi, Z.G. Zhang, K. Hellgardt, K. Honda, T. Yoshida, Catal. Today 77 (2002) 181.
[20] V.R. Choudhary, B.S. Uphade, A.S. Mamman, Appl. Catal. A Gen. 168 (1998) 33.
[21] P.D.F. Vernon, M.L.H. Green, A.K. Cheetham, A.T. Ashcroft, Catal. Today 13 (1992) 417.
[22] S. Liu, G. Xiong, H. Dong, W. Yang, Appl. Catal. A Gen. 202 (2000) 141.
[23] A.M. O'Connor, J.R.H. Ross, Catal. Today 46 (1998) 203.
[24] V.R. Choudhary, A.M. Rajput, B. Prabhakar, Catal. Lett. 32 (1995) 391.
[25] T. Inui, K. Saigo, Y. Fujii, K. Fujioka, Catal. Today 26 (1995) 295.
[26] V.R. Choudhary, A.M. Rajput, Ind. Eng. Chem. Res. 35 (1996) 3934.
[27] V.R. Choudhary, A.S. Mamman, Appl. Energy 66 (2000) 161.
[28] B.T. Li, K. Maruyama, M. Nurunnabi, K. Kunimori, K. Tomishige, Appl. Catal. A Gen. 275 (2004) 157.
[29] K. Takehira, T. Shishido, D. Shoro, K. Murakami, M. Honda, T. Kawabata, K. Takaki, Catal. Commun. 5 (2004) 209.
[30] J.A.C. Dias, J.M. Assaf, J. Power Sources 130 (2004) 106.
[31] K. Takehira, T. Shishido, P. Wang, T. Kosaka, K. Takaki, J. Catal. 221 (2004) 43.
[32] S. Freni, G. Calogero, S. Cavallaro, J. Power Sources 87 (2000) 28.
[33] B.T. Li, K. Maruyama, M. Nurunnabi, K. Kunimori, K. Tomishige, Ind. Eng. Chem. Res. 44 (2005) 485.
[34] T.B. Reed, Free Energy Formation of Binary Compounds, MIT Press, Cambridge, 1971.
[35] O. Yamazaki, K. Tomishige, K. Fujimoto, Appl. Catal. A Gen. 136 (1996) 49.
[36] K. Tomishige, Y. Himeno, Y. Matsuo, Y. Yoshinaga, K. Fujimoto, Ind. Eng. Chem. Res. 39 (2000) 1891.
[37] K. Tomishige, Y.G. Chen, K. Fujimoto, J. Catal. 181 (1999) 91.
[38] C.H. Bartholomew, R.B. Pannell, J.L. Butler, J. Catal. 65 (1980) 335.
[39] F. Arena, B.A. Horrell, D.L. Cocke, A. Parmaliana, N. Giordano, J. Catal. 132 (1991) 58.
[40] Z. Hu, T. Wakasui, A. Maeda, K. Kunimori, T. Uchijima, J. Catal. 127 (1991) 276.
[41] W.L. Bragg, The Crystalline State, G. Bell, London, 1933.
[42] R. Molina, G. Poncelet, J. Catal. 173 (1998) 257.
[43] W.S. Dong, H.S. Roh, K.W. Jun, S.E. Park, Y.S. Oh, Appl. Catal. A Gen. 226 (2002) 63.
[44] S.B. Wang, G.Q. Lu, Appl. Catal. A Gen. 169 (1998) 271.